International Symposium
On Turbulence and Shear Flow
Phenomena (TSFP-9)
June 30 - July 3, 2015 *Melbourne, Australia*

PITM SIMULATION OF THE TURBULENT FLOW IN A SMALL AXISYMMETRIC CONTRACTION

Bruno Chaouat
Department of Computational Fluid Dynamics
ONERA
BP 72 - 92322 Châtillon cedex, France
bruno.chaouat@onera.fr

ABSTRACT

We perform a numerical simulation of the turbulent flow in a small axisymmetric contraction using a subfilter scale stress model derived from the partially integrated transport modeling (PITM) method. Relatively to the experiment, to reproduce the effects of the square-mesh biplane grid on the uniform wind tunnel stream, we generate the inflow condition by means of an analytical pseudo-random field in a cubic box that is introduced in the inlet section of the channel. As a result, it is found that the simulation predicts fairly well this turbulent flow. As expected, the initial anisotropy is reduced in the contraction. Moreover, as a promising result, the "return to anisotropy " occurring after the contraction in the straight duct section is well recovered according to the experiment. This work shows that the PITM method used in conjunction with an analytical synthetic turbulence generation as inflow is well suited for simulating this flow and allows an understanding of the physical mechanisms acting in an axisymmetric contraction.

INTRODUCTION

Turbulent flow subjected to an axisymmetric contraction in the streamwise direction is encountered in many engineering applications. As known, the effect of contraction on the mean flow and on the turbulence is mainly to accelerate the flow and to reduce the flow anisotropy while the flow structures are appreciably modified when passing through the contraction due to vortex stretching and rotation (Uberoi and Wallis, 1966; Sjogren and Johansson, 1998; Jang et al., 2011) . Several authors, Uberoi and Wallis (1966), Comte-Bellot and Corrsin (1966) , as well as Bernett and Corrsin (1978) studied the effects of grid-generated turbulence in a small contraction ranging from 1.19 to 1.41. In this framework, the latter experiment of Uberoi and Wallis (1966) deserves a particular interest because it presents a complex phenomena in physics of fluid turbulence that still raises some questions of interpretation in term of turbulence. In this experiment, initial fluid particles are convected into a channel through a square-mesh biplane grid and are then subjected to a sudden contraction. The effect of the square mesh biplane grid made of round wooden rods on the uniform stream flow was to generate an anisotropic turbulence just downstream the grid. Just behind the grid, the streamwise fluctuating velocity correlations was $\tau_{22} = \tau_{33} \approx \tau_{11}/1.4$. The measurements indicated that this ratio τ_{11}/τ_{22} initially closes to 1.4 returned to unity through the contraction because of the rapid deformation of the mean flow. But after the contraction in the straight duct section, this ratio however gradually reincreased to its pre-contraction value. This phenomena constitutes a paradox which still deserves interest in physics of fluid turbulence. The objective is then to investigate this complex flow in a small contraction by performing a numerical simulation using the partially integrated transport modeling (PITM) method including a second moment closure developed by Chaouat and Schiestel, (2005, 2009) in conjunction with an analytical synthetic turbulence generation for inflow conditions. Indeed, instead of computing the fine grained turbulence around the grid which is too costly in term of computing time and memory resources, we develop a specific method to generate an anisotropic analytical pseudo-random field. This artificial field is created in a cubic box that is pushed into the computational domain to produce the inlet conditions of the computational domain.

WIND TUNNEL EXPERIMENT

Experimental results

The wind tunnel used in the experiment of Uberoi and Wallis (1966) is sketched in figure 1. The dimension of the square-mesh biplane grid is $D_1 = 60.96$ cm whereas the dimension of the wind tunnel in the longitudinal direction is $L_1 = 254$ cm. The small axisymmetric contraction of the wind tunnel cross-section is of ratio $C = A_1/A_2 = 1.25$, where A_1 and A_2 denote the section areas before and after the contraction. The Reynolds number $Re = U_b D_1/\nu$ based on the bulk velocity U_b, the height D_1 and the kinematic viscosity ν takes on the value $Re \approx 4.47\,10^5$. Third set of experiments (Uberoi and Wallis, 1966) were performed with a first square-mesh biplane grid of 5.08 cm made of round wooden rods of 1.27 cm diameter, a second square-mesh grid of 2.54 cm made of rods of 0.635 cm diameter and also a third square-mesh grid of 1.27 cm made of rods of 0.3175 cm diameter corresponding to the Reynolds numbers $R_M = U_b M/\nu = 9300$, 18 600 and 37 200, respectively, where M denotes the mesh size of the grid (5.08 cm, 2.54 cm and 1.27 cm). As a result, it was found that the effect of a fixed contraction on the turbulence decreases with decreasing mesh size of the grid and that for all cases, the initial ratio of the stress components τ_{11}/τ_{22} close to 1.4 behind the grid gradually decreases in the axisymmetric contraction and reincreases after passing through the axisymmetric contraction in the uniform straight section. This outcome

was observed for all grids of three mesh sizes M.

Grid-turbulence

In the present case, we focus interest on the case $R_M = 37.2\ 10^2$ because of its higher contraction effects on the turbulence. In the experiment, the largest scales in the grid-generated turbulence are essentially determined by the mesh size of the grid M whereas the smallest scales are fixed by the Kolmogorov law. The ratio $\alpha = 10^{-3}U_b^2/\tau_{11}$ and $\beta = 10^{-3}U_b^2/\tau_{22}$, as well as the ratio of the streamwise turbulent stress to the spanwise turbulent stress $\gamma = \tau_{11}/\tau_{22}$ are measured in the center of the channel at different grid Reynolds numbers R_M. The state of turbulence just behind the grid is then determined from the experiment suggesting that $\alpha = 10^{-3}U_b^2/\tau_{11} = 0.3$, $(\tau_{11}/U_b^2 = 0.33\,\%)$, just after the grid. As the ratio $\gamma = \tau_{11}/\tau_{22} \approx 1.4$, the turbulent energy is easily computed as $k_0 = 0.49$ m^2/s for the bulk velocity $U_b = 11.0$ m/s. The dissipation-rate is determined by the Reynolds number from the relation $R_t = k^2/\nu\varepsilon$. Considering the experiments of Comte-Bellot and Corrsin (1966) , and Sjögren and Johansson (1998) , the Reynolds number is set to 1600 implying that the dissipation rate takes on the value 10.0 m^2/s^3 for $\nu = 1.50\,10^{-5}$ m^2/s. The frequency is then $\varepsilon_0/k_0 = 20.4$ s^{-1}. The Kolmogorov scale η_0 computed as $\eta_0 = (\nu^3/\varepsilon_0)^{1/4}$ is 0.135 mm whereas the large scale computed as $L_0 = k_0^{3/2}/\varepsilon_0$ is close to 3.43 cm which is of the same order of the mesh size M of the experimental biplane grid (5.08 cm, 2.54 cm and 1.27 cm).

NUMERICAL SIMULATION

Filtering process and governing equations

In PITM, as for large eddy simulations, any flow variable ϕ is decomposed into a large or resolved scale $\bar{\phi}$ and a subfilter or modeled scale $\phi^>$. As usually, the filtered variable $\bar{\phi}$ is defined by the filtering operation as the convolution with a filter G in space $\overline{\phi} = G * \phi$ that leads to the computation of a variable convolution integral

$$\bar{\phi}(x,t) = \int_{\mathbb{R}^3} G[x-\xi,\Delta]\,\phi(\xi,t)d\xi \tag{1}$$

where Δ denotes the filter-width. In view of the statistical averaging process, the instantaneous variable ϕ can also be decomposed into a statistical mean part $\langle\phi\rangle$ and a fluctuating part ϕ' leading to $\phi = \langle\phi\rangle + \phi'$. The instantaneous fluctuation ϕ' includes in fact the large scale fluctuating part $\phi^<$ and the small scale fluctuating part $\phi^>$ such that $\phi' = \phi^< + \phi^>$. So that ϕ can then be rewritten as the sum of a mean statistical part $\langle\phi\rangle$, a large scale fluctuating part $\phi^<$ and a small scale fluctuating part $\phi^>$ as follows $\phi = \langle\phi\rangle + \phi^< + \phi^>$. The first two terms correspond to the filtered velocity $\bar{\phi} = \langle\phi\rangle + \phi^<$ implying that the large scale fluctuating part is simply the difference between the filtered and the statistical quantities, $\phi^< = \bar{\phi} - \langle\phi\rangle$. The filtering of the instantaneous Navier-Stokes equation produces the resolved scale motion as follows, provided the commutation terms are negligible (Chaouat and Schiestel, 2013)

$$\frac{\partial\bar{u}_i}{\partial t} + \frac{\partial(\bar{u}_i\bar{u}_j)}{\partial x_j} = -\frac{1}{\rho}\frac{\partial\bar{p}}{\partial x_i} + \nu\frac{\partial^2\bar{u}_i}{\partial x_j\partial x_j} - \frac{\partial(\tau_{ij})_{sfs}}{\partial x_j} \tag{2}$$

where u_i, p, ν, $(\tau_{ij})_{sfs}$, are the velocity vector, the pressure, the molecular viscosity and the subfilter-scale stress tensor, respectively. The subfilter-scale tensor $(\tau_{ij})_{sfs}$ is defined by the mathematical relation $(\tau_{ij})_{sfs} = \overline{u_iu_j} - \bar{u}_i\bar{u}_j$. The presence of the turbulent contribution $(\tau_{ij})_{sfs}$ in equation (2) indicates the effect of the subfilter scales on the resolved field. The resolved scale tensor is defined by the relation $(\tau_{ij})_{les} = \bar{u}_i\bar{u}_j - \langle u_i\rangle\langle u_j\rangle$. The Reynolds stress tensor τ_{ij} including the small and large scale fluctuating velocities can be computed as a first approximation as the sum of the subfilter and the resolved stress tensors $\tau_{ij} = \langle(\tau_{ij})_{sfs}\rangle + \langle(\tau_{ij})_{les}\rangle$ whereas the statistical turbulent kinetic energy is obtained as the half-trace of the stress tensor τ_{ij} leading to $k = \langle k_{sfs}\rangle + \langle k_{les}\rangle$. Closure of the momentum equation is necessary for the subfilter turbulent stress tensor $(\tau_{ij})_{sfs}$ which is modeled by means of its transport equation.

PITM method

Principle of the method

The PITM method allows to perform hybrid non-zonal RANS/LES simulations of turbulent flows (Schiestel and Dejoan, 2005; Chaouat and Schiestel, 2005; Chaouat, 2012) on coarse grids when the cutoff wave number associated with the grid size can be placed before the inertial zone as far as the grid size is however sufficient to describe correctly the mean flow. In the present case, as the flow anisotropy is a central subject of investigation, we apply the subfilter scale stress transport model derived from PITM which is based on a second moment closure (SMC) to perform this wind-tunnel flow. This model relies on the transport equations for the subfilter-scale stresses $(\tau_{ij})_{sfs}$ and dissipation rate ε_{sfs} (seven equations) and constitutes therefore in its formulation one of the most advanced model used in hybrid RANS/LES simulations (Fröhlich and Von Terzi, 2008) . The model is governed by some functions of the dimensionless cutoff parameter $\eta_c = \kappa_c L_e$ involving the cutoff wave number $\kappa_c = \pi/\Delta$ and the integral turbulent length scale $L_e = k^{3/2}/\varepsilon$, built using the total turbulent kinetic energy $k = \langle k_{sfs}\rangle + \langle k_{les}\rangle$, the total dissipation rate $\varepsilon = \langle\varepsilon_{sfs}\rangle + \langle\varepsilon^<\rangle$, itself composed of the subfilter transfer rate ε_{sfs} and the resolved large scale dissipation rate $\varepsilon^<$. So, the PITM equations describe the physical turbulent processes involving the production, dissipation and flux transfer of the partial turbulent energy associated with each spectral zone $[0,\kappa_c]$, $[\kappa_c,\kappa_d]$ and $[\kappa_d,\infty[$ where κ_c and κ_d denote the cutoff wave number and dissipative wave number, respectively, and can be interpreted as spectral balance equations.

Subfilter scale stress transport equation

The transport equation for the subfilter stress tensor can be written in the simple compact form as

$$\frac{\partial(\tau_{ij})_{sfs}}{\partial t} + \frac{\partial}{\partial x_k}\left(\bar{u}_k(\tau_{ij})_{sfs}\right) = P_{ij} + \Pi_{ij} + J_{ij} - \frac{2}{3}\delta_{ij}\varepsilon_{sfs} \tag{3}$$

where the terms appearing in the right-hand side of this equation are identified here as subfilter production, redistribution, diffusion and dissipation, respectively. The production term P_{ij} accounts for the interaction between the stresses and the filtered velocity gradients

$$P_{ij} = -(\tau_{ik})_{sfs}\frac{\partial\bar{u}_j}{\partial x_k} - (\tau_{jk})_{sfs}\frac{\partial\bar{u}_i}{\partial x_k} \tag{4}$$

The redistribution term Π_{ij} appearing in equation (3) is modeled by considering its corresponding modeling in RANS methodology. This modeling implicitly assumes that the interaction mechanisms of the subgrid scales with the resolved scales of the turbulence is of the same nature than the interaction mechanisms involving all the fluctuating scales with the main flow. However, since the small scales return more rapidly to isotropy than the large scales, the slow redistribution term Π^1_{ij} increases with the cutoff wave number κ_c in order to strengthen the return to isotropy for large wave numbers. This argument was previously adopted in multiple-scale models (Schiestel, 1987) considering that the return to isotropy is of higher intensity in the spectral range of high wave numbers. Taking into account these arguments, the redistribution term Π_{ij} is decomposed into a slow part Π^1_{ij} that characterizes the return to isotropy due to the action of turbulence on itself

$$\Pi^1_{ij} = -c_{1sfs}\frac{\varepsilon_{sfs}}{k_{sfs}}\left((\tau_{ij})_{sfs} - \frac{1}{3}(\tau_{mm})_{sfs}\delta_{ij}\right) , \quad (5)$$

and a rapid part, Π^2_{ij} that describes the action of the filtered velocity gradients

$$\Pi^2_{ij} = -c_2\left(P_{ij} - \frac{1}{3}P_{mm}\,\delta_{ij}\right) , \quad (6)$$

where c_{1sfs} plays the same role as the Rotta coefficient but is no longer constant whereas c_2 is the same coefficient used in RANS modeling. In practice, the function c_{1sfs} is modeled as $c_{1sfs} = c_1\alpha(\eta)$ where c_1 is the usual Rotta constant coefficient used in statistical modeling and α is an increasing function of the parameter η. The diffusion terms J_{ij} is modeled assuming a well-known gradient law

$$J_{ij} = \frac{\partial}{\partial x_m}\left(\nu\frac{\partial(\tau_{ij})_{sfs}}{\partial x_m} + c_s\frac{k_{sfs}}{\varepsilon_{sfs}}(\tau_{ml})_{sfs}\frac{\partial(\tau_{ij})_{sfs}}{\partial x_l}\right) \quad (7)$$

where c_s is a constant coefficients.

Subfilter scale dissipation-rate transport equation

Equation (3) needs to model the subfilter scale dissipation-rate ε_{sfs} at high Reynolds number. This modeling is made by means of its transport equation that reads

$$\frac{\partial\varepsilon_{sfs}}{\partial t} + \frac{\partial}{\partial x_k}\left(\bar{u}_k\varepsilon_{sfs}\right) = c_{sfs\varepsilon_1}\frac{\varepsilon_{sfs}}{k_{sfs}}P - c_{sfs\varepsilon_2}\frac{\varepsilon^2_{sfs}}{k_{sfs}} + J_\varepsilon \quad (8)$$

where J_ε denotes the diffusion term. In equation (8), the coefficient $c_{sfs\varepsilon_1}$ appearing in the source term of the dissipation-rate equation is the same as the one used in the corresponding RANS dissipation equation $c_{sfs\varepsilon_1} = c_{\varepsilon_1}$ whereas the coefficient $c_{sfs\varepsilon_2}$ appearing in the destruction term of the dissipation-rate equation is now given by

$$c_{sfs\varepsilon_2} = c_{\varepsilon_1} + \frac{\langle k_{sfs}\rangle}{k}(c_{\varepsilon_2} - c_{\varepsilon_1}) \quad (9)$$

where c_{ε_1} and c_{ε_2} are the constant coefficient used in the statistical RANS dissipation-rate equation. The ratio $\langle k_{sfs}\rangle/k$ appearing in equation (9) is evaluated by reference to an analytical energy spectrum $E(\kappa)$ inspired from a Von Kármán spectrum considered as a limiting equilibrium distribution leading to the result

$$c_{sfs\varepsilon_2}(\eta_c) = c_{\varepsilon_1} + \frac{c_{\varepsilon_2} - c_{\varepsilon_1}}{\left[1+\beta_\eta\,\eta_c^3\right]^{2/9}} \quad (10)$$

Equation (10) indicates that the parameter η_c acts like a dynamic parameter which depends on the location of the cutoff wave number κ_c within the energy spectrum and the value of the function $c_{sfs\varepsilon_2}$ then controls the relative amount of turbulence energy contained in the subfilter range. The theoretical value of the coefficient β_η in equation (10) is $\beta_\eta = [2/(3C_K)]^{9/2}$ where C_K is the Kolmogorov constant (Chaouat and Schiestel, 2009) . The diffusion term $(J_\varepsilon)_{sfs}$ is modeled by a gradient tensorial law

$$J_\varepsilon = \frac{\partial}{\partial x_j}\left(\nu\frac{\partial\varepsilon_{sfs}}{\partial x_j} + c_\varepsilon\frac{k_{sfs}}{\varepsilon_{sfs}}(\tau_{jm})_{sfs}\frac{\partial\varepsilon_{sfs}}{\partial x_m}\right) \quad (11)$$

where c_ε is a constant coefficient.

Inlet condition

The flow conditions are nominally atmospheric air. The simulation of the flow around the square-mesh biplane grid made on round wooden rods (Uberoi and Wallis, 1966) is difficult to perform numerically because of the three dimensional geometry of the grid that requires a specific work in mesh generation. In addition, the simulation of the flow details around the fine grid is extremely costly in term of computational resources, both for the number of grid-points and computer time. Taking into account these constraints, we prefer to create an anisotropic pseudo-random turbulence field characterized by its anisotropy condition as $\tau_{22} = \tau_{33} \approx \tau_{11}/1.4$ by means of an analytical method to produce the inlet conditions. This procedure consists in generating a complete tridimensional flow in a cubic box at a given time that is then progressively moved at the inlet of the computational domain of the wind-tunnel with a constant convection velocity corresponding to the uniform stream flow of the experiment. The instantaneous variables including the velocity and the turbulent stresses of the flow field in the entrance of the computational domain are then interpolated in space discretization from the box flow solution. Because of the long time simulation that is necessary to reach for computing the statistics, several cubes are in fact generated, independently from each other, and enforced in the axisymmetric contraction domain. A thorough review on methods of generation of synthetized turbulence has been conducted recently by Shur et *al.* (2014) . In the present case, we consider the method of Roy (1980) initially developed for isotropic fields and we extend it to account for anisotropic fields by applying a transformation vector on the isotropic vector stream function (Befeno and Schiestel, 2007) . The first step consists in generating an homogeneous isotropic field, uniformly distributed on a sphere of radius unity in the spectral space by means of a random vector stream function $\hat{\psi}(\kappa)$. The fluctuating velocity is then obtained from the stream function as $\hat{u} = \kappa \wedge \hat{\psi}$ with specific conditions imposed on ψ to satisfy the energy equation with a given density energy $E(\kappa)$ imposed. The second

step consists in applying a second order tensor β operating on the isotropic vector field to produce the anisotropic flow field. As a result, the velocity in the spectral space is then given by $\hat{u}(\kappa) = \kappa \wedge \beta\,\hat{\psi}(\kappa)$ implying that the continuity equation is still preserved. The tensor β is determined by means of algebra calculus in the spectral space to get the desired anisotropic resolved field. The starting point consists in applying another tensor transformation α on the velocity itself leading to $\hat{u}(\kappa) = \alpha(\kappa \wedge \hat{\psi}(\kappa))$. The tensor β is then expressed as a function of α. The resulting equation finally reads $\hat{u}(\kappa) = \alpha(\kappa \wedge \hat{\psi}(\kappa)) = \kappa \wedge \beta\,\hat{\psi}(\kappa)$ or for the i component, $\hat{u}_i = j\kappa_j \alpha_{im} \varepsilon_{mjk} \hat{\psi}_k = j\varepsilon_{ijk}\kappa_j \beta_{km} \hat{\psi}_m$. The spectral turbulent energy associated with the wave number κ is then given by $\langle u(\kappa) u^*(\kappa)\rangle$. To reproduce the axisymmetric turbulence of the Uberoi and Wallis experiment, it is found that $\beta_{22} = \beta_{33}$ and $\beta_{11}/\beta_{22} < 1$. Finally, we take the spherical mean $\mathscr{M}$ (Jeandel et al., 1978)

$$\mathscr{M}(\psi(\kappa)) = \frac{1}{\mathscr{A}} \int\int_{\mathscr{A}} \psi(\kappa)\, d\mathscr{A} \tag{12}$$

of the equations, where $\mathscr{A}$ denotes the area element on the sphere of radius $\kappa = |\kappa|$, to get quantities which are not depending on the wave number. Setting $\beta_{11} = 1 - 2\gamma$, $\beta_{22} = 1 + \gamma$, $\beta_{33} = 1 + \gamma$, we show that γ is then solution of a second degree equation and its exact value is obtained by successive approximations. The resolved scale stress as a function of the cutoff wave number κ_c given by the grid-size of the box is then computed from integration of the spectral Reynolds stress tensor as follows

$$\tau_{ij} = \int\int\int \left\langle \hat{u}_i(\kappa) \hat{u}_j^*(\kappa) \right\rangle d^3\kappa \tag{13}$$

The subfilter scale stresses are computed by a viscosity model using the Boussinesq hypothesis verifying also the anisotropy condition. So that, the resolved and subgrid turbulent fields are built in order to satisfy the anisotropy condition from a statistical point of view in the whole cubic domain at a given time for all turbulence scales.

Wall condition

No slip boundary conditions are imposed at the walls. To get accurate results, the wall sublayers are fully calculated by the turbulence model at low Reynolds number without requiring any empirical law of the wall.

NUMERICAL METHOD AND CONDITIONS OF COMPUTATIONS

The present numerical simulation solves the filtered Navier-Stokes equation and seven transport equations for the subfilter scale stress tensor $(\tau_{ij})_{sfs}$ and dissipation rate ε_{sfs}. The equations are integrated in time using an explicit Runge-Kutta scheme of fourth-order accuracy along with an implicit iterative scheme for the source terms. The convective fluxes at the cell interfaces resulting from the volume technique are computed by an approximate Riemman solver of fourth-order accuracy in space. The simulation is performed on a coarse curvilinear mesh $100 \times 70 \times 70$ grid points in the streamwise x_1 and lateral directions (x_2, x_3). The use of a coarse grid is deliberate choice because the aim is precisely to appreciably reduce the computational cost while obtaining satisfying accurate solution. Note that in the present case, highly resolved large eddy simulation using viscosity models is out of reach because of the large dimension of the channel $L_1 = 2.54$ m and the high Reynolds number of the flow $Re \approx 4.47\,10^5$. The statistics of the PITM simulation are obtained by averaging in time the instantaneous flow accounting for roughly five convective time scale $T = D_1/U_b$ where U_b is the bulk velocity.

NUMERICAL RESULTS

Inlet turbulence field

The anisotropic turbulence is performed on a cubic box of dimension $D_1 = 0.6096$ m accounting for $N = 68^3$ grid-points. The wave numbers are defined by $\kappa_m = 2\pi/m$ where m varies in the range $[-N/2+1, N/2]$ leading to a minimum wave number $\kappa_{min} = 10.13\ m^{-1}$ and $\kappa_{max} = \pi/\Delta = 344.5\ m^{-1}$. However, the effective wave number retained in the present case is $\kappa_c = 103\ m^{-1}$ to suppress high frequencies of the fluctuating velocities. It is found that the parameter γ introduced in the matrix β takes on the value $\gamma = 0.198$ to get the desired anisotropy turbulent field. Figure 2 shows the vortical activity of the synthetic turbulence for the anisotropic field verifying $\tau_{11}/k = 0.823$, $\tau_{22}/k = 0.588$, $\tau_{33}/k = 0.588$. The isosurfaces are illustrated by the Q criterion defined as $Q = \frac{1}{2}(\Omega_{ij}\Omega_{ij} - S_{ij}S_{ij})$ corresponding to the balance between the local rotation rate Ω and the strain rate S of the velocity. Although the turbulent field is artificial, i.e., not a solution of the Navier-Stokes equations, one can observe at a first sight the presence of vortical elongated structures associated with the large scales.

Key features of the axisymmetric contraction

Turbulent flow structures Figure 1 shows the Q isosurfaces of the flow performed on the coarse mesh illustrating the vortical activity and the instantaneous flow structures. As expected, the vortical activity is of higher intensity in the contracting zone than in the straight section of the channel because of the effect of contraction on the velocity gradients. Moreover, the flow structures appear more elongated after the contraction.

friction coefficients Figure 3 displays the evolution of the friction coefficient $C_f = \tau_w/(0.5\rho U_b^2)$ along the wall in the streamwise direction. It can be seen that the friction coefficient slightly decreases in the straight entrance section of the channel. It highly increases in the contracting zone and decreases rapidly just after the contraction. Then, it gradually decreases again in the straight section of the channel towards the exit. As this coefficient takes on positive value, one can deduce that the contraction value $C = 1.25$ is too small to induce the detachment of the boundary layer.

Velocity and turbulent stresses Figure 4 exhibits the mean velocity profiles versus the channel height at several locations of the channel before the contraction at $x_1/D_1 = 0.2$ and after the contraction at $x_1/D_1 = 2$. The flatness of the mean velocity due to the turbulence effect is well marked. According to the contraction value $C = 1.25$, the mean dimensionless velocity goes from unity to 1.25 when passing the contraction. Figure 5 displays the evolution of the streamwise and lateral Reynolds stresses normalized by the bulk velocity τ_{11}/U_b^2 and τ_{33}/U_b^2, respectively,

at the same locations illustrating the effect of the axisymmetric contraction on the turbulence. Just after the contraction, the flow reaches an isotropy state of turbulence characterized by $\tau_{ij} = 2/3k\delta_{ij}$. Apart from the wall region that reveals the presence of turbulent peaks of turbulence, the stress profiles are almost uniform in the cross sections indicating that the flow can be considered as locally homogeneous.

Flow anisotropy Figure 6 shows the evolution of the dimensionless bulk velocity U_b^* and the ratio of the turbulent stresses τ_{11}/τ_{22}, respectively, along the centerline of the channel in the streamwise direction both for the RANS computation using the Reynolds stress model (Launder and Shima, 1989) and for the PITM simulation. For PITM, note that the turbulent stress τ_{ij} is computed as the sum of the subgrid and resolved stresses. As observed in the preceding section, the effect of the axisymmetric contraction is well visible on the dimensionless bulk velocity which goes from unity to 1.25 after the contraction. As expected, the RSM model here based on a single-scale of turbulence is unable to reproduce the reincrease of anisotropy after the contraction. In RANS methodology, only multiple-scale modeling succeeded to reproduce this effect (Schiestel, 1987) . In the present case, it appears that the PITM simulation provides a ratio anisotropy τ_{11}/τ_{22} that agrees relatively well with the experimental data. More precisely, the ratio initially closes to 1.4 goes to unity through the contraction because of the rapid deformation due to the mean flow and returns to its pre-contraction value in the straight duct section. This phenomena of the return to anisotropy can be explained by the relaxation process of the turbulence scales. In the contraction, the turbulence is isotropic because the large scale and small scale anisotropies are just compensating. When passing from the contraction to the straight section of the channel, the small scale motions return more rapidly to isotropy than the large scales, so that the anisotropy of the large scale that was temporarily hidden by the small scales before the contraction reappears. This interpretation of scale effect is currently investigated by means of scale separation of the turbulent flow along the centerline of the channel.

CONCLUSION

A numerical simulation of the turbulent flow in the small axisymmetric contraction of the wind tunnel designed by Uberoi and Wallis using the subfilter scale stress model derived from the partially integrated transport modeling (PITM) method has been performed on a coarse mesh. In conjunction with the turbulence model, a random velocity field has been used to generate the inlet turbulence especially with the aim to reproduce the effects of the square-mesh biplane grid on the uniform wind tunnel stream. As a result, it is has been found that the PITM simulation, although performed on a coarse mesh, predicts this flow fairly well in good agreement with the experiment. In particular, PITM was able to reproduce the reincrease of the anisotropy ratio τ_{11}/τ_{22} in the straight section along the centerline of the channel after the contraction.

REFERENCES

Befeno, I. & Schiestel, R. 2007 Non-equilibrium mixing of turbulence scales using a continuous hybrid RANS/LES approach: Application to the shearless mixing layer. *Flow, Turbulence and Combustion* **78**, 129–151.

Bennet, J. C. & Corrsin, S. 1978 Small Reynolds number nearly isotropic turbulence in a straight duct and a contraction. *Physics of Fluids* **21** (12), 2129–2140.

Chaouat, B. 2012 Simulation of turbulent rotating flows using a subfilter scale stress model derived from the partially integrated transport modeling method. *Physics of Fluids* **24** (045108), 1–35.

Chaouat, B. & Schiestel, R. 2005 A new partially integrated transport model for subgrid-scale stresses and dissipation rate for turbulent developing flows. *Physics of Fluids* **17** (065106), 1–19.

Chaouat, B. & Schiestel, R. 2009 Progress in subgrid-scale transport modelling for continuous hybrid non-zonal RANS/LES simulations. *International Journal of Heat and Fluid Flow* **30**, 602–616.

Chaouat, B. & Schiestel, R. 2013 Partially integrated transport modeling method for turbulence simulation with variable filters. *Physics of Fluids* **25** (125102), 1–39.

Comte-Bellot, G. & Corrsin, S. 1966 The use of a contraction to improve the isotropy of grid-generated turbulence. *Journal of Fluid Mechanics* **25**, 657–682.

Fröhlich, J. & Terzi, D. Von 2008 Hybrid LES/RANS methods for the simulation of turbulent flows. *Progress in Aerospace Sciences* **44** (5), 349–377.

Jang, S. J., Sung, H. J. & Krogstad, P. 2011 Effects on a axisymmetric contraction on a turbulent pipe flow. *Journal of Fluid Mechanics* **687**, 376–403.

Jeandel, D., Brison, J. F. & Mathieu, J. 1978 Modeling methods in physical and spectral space. *Physics of Fluids* **21** (2), 169–182.

Launder, B. E. & Shima, N. 1989 Second moment closure for the near wall sublayer: Development and application. *AIAA Journal* **27** (10), 1319–1325.

Roy, Ph. 1980 Résolution des équations de Navier-Stokes par un schéma de haute précision en espace et en temps. *La Recherche Aérospatiale* **6**, 373–385.

Schiestel, R. 1987 Multiple-time scale modeling of turbulent flows in one point closures. *Physics of Fluids* **30** (3), 722–731.

Schiestel, R. & Dejoan, A. 2005 Towards a new partially integrated transport model for coarse grid and unsteady turbulent flow simulations. *Theoretical Computational Fluid Dynamics* **18**, 443–468.

Shur, M. L., Spalart, P. R. & Travin, M. K. Strelets A. K. 2014 Synthetic turbulence generators for RANS-LES interfaces in zonal simulations of aerodynamic and aeroacoustic problems. *Flow, Turbulence and Combustion* **93**, 63–92.

Sjögren, T. & Johansson, A. 1998 Measurement and modelling of homogeneous axisymmetric turbulence. *Journal of Fluid Mechanics* **374**, 59–89.

Uberoi, M. S. & Wallis, S. 1966 Small axisymmetric contraction of grid turbulence. *Journal of Fluid Mechanics* **24**, 539–543.

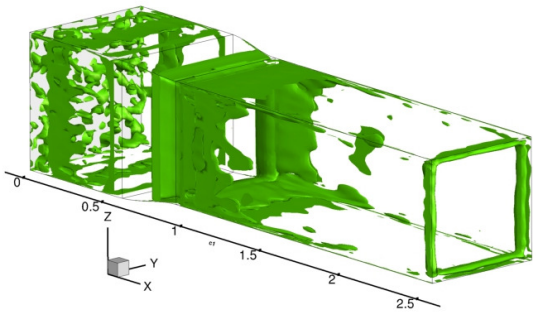

Figure 1. Vortical activity illustrated by the Q isosurfaces at $Re = 4.4\,10^5$. PITM simulation $100 \times 70 \times 70$. View of the small axisymmetric contracted channel in real aspect ratio Uberoi & Wallis (1966) ($L_1 = 2.54$ m, $D_1 = 0.61$ m, $C = A_1/A_2 = 1.25$).

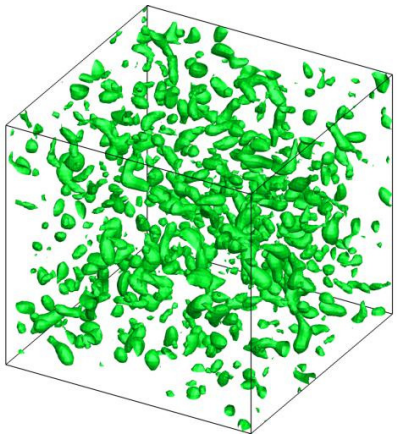

Figure 2. Figure 3: View of the anisotropic turbulent field generated in a cube. Vortical activity illustrated by the Q isosurfaces.

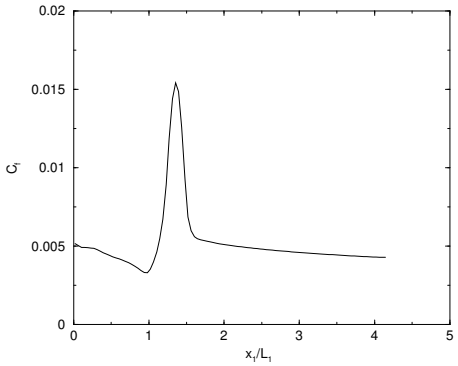

Figure 3. Friction coefficient $C_f = \tau_w/(0.5\rho U_b^2)$ along the wall at $Re = 4.47\,10^5$.

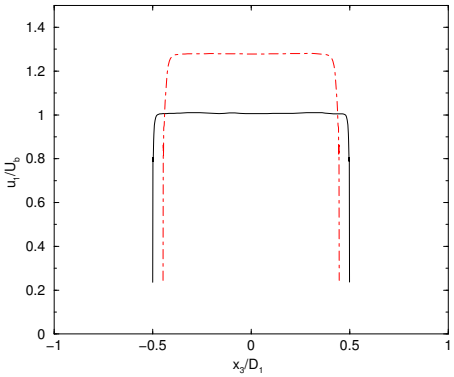

Figure 4. Mean velocity u_1/U_b at various locations $x_1/D_1 = 0.2$: —; $x_1/D_1 = 2$: .-.-.

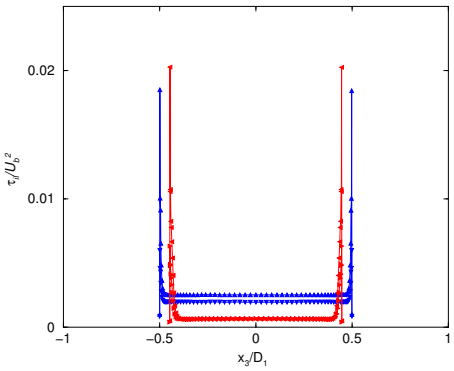

Figure 5. Reynolds stress τ_{ii}/U_b^2 at various locations $x_1/D_1 = 0.2$: (i=1) ▲; (i=2) ▼. $x_1/D_1 = 2$: (i=1) ◀; (i=2) ▶.

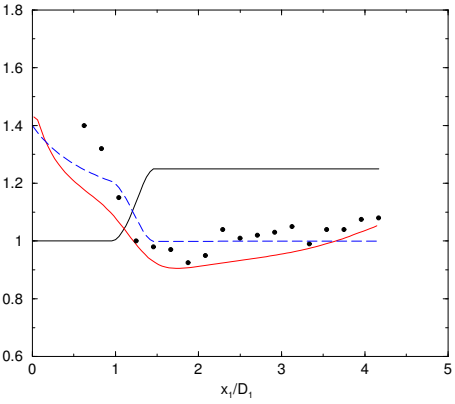

Figure 6. Evolution of the dimensionless bulk velocity $U_b^*(x_1)$, and the ratio τ_{11}/τ_{22} on the centerline of the channel in the streamwise direction. Experiment ∘ Uberoi & Wallis (1966). single-scale RSM model .-.-.; PITM —; $Re = 4.47\ 10^5$